Combined Planar Measurements of Flow Velocity and Mass Concentration in Shallow Turbulent Flow Part 2: Application of coupled PIV-PCA to Turbulent Shallow Wake Flows

Carl Fr. v.Carmer, Andreas C. Rummel & Gerhard H. Jirka
Institute for Hydromechanics, University of Karlsruhe, 76128 Karlsruhe, Germany
carmer@ifh.uka.de, rummel@ifh.uka.de, jirka@ifh.uka.de

Abstract: In order to examine the instability mechanisms in shallow turbulent shear flow, a large and well equipped shallow water test facility has been constructed at the Institute for Hydromechanics, University of Karlsruhe. In this 5.5 m wide and 13.5 m long basin - operated at water depths of only a few centimeters - a plane turbulent equilibrium shear flow is produced. In the present study a disturbance is induced to the base flow by forcing it to flow around a single cylindrical body with a diameter D, which is clearly larger than the water depth h. This destabilization results in a vortex street-like shallow turbulent wake flow. A Particle Image Velocimetry (PIV) measuring technique using particles floating at the free surface is employed to obtain horizontal velocity fields, and a Planar Concentration Analysis (PCA) method processing digitized video frames provides depth-averaged concentration fields. A phase-resolved averaging procedure based on individually variable cycle periods is applied to extract the periodic 'coherent' flow. Large-scale coherent vortical structures can directly be identified from the coherent motion using an eduction scheme, which distinguishes between vorticity- and strain-dominated flow regions. After adjustment and cross-correlation the phase-resolved averaged fields of velocity and tracer mass from the PIV and PCA measurements reveal the transport capacity of these large-scale structures for momentum and mass.

Introduction

Turbulent shallow flows having a limited vertical extent in a horizontally unbounded domain are ubiquitous in our environment, e.g. wide rivers, lakes, estuaries, shallow coastal waters or the stratified atmosphere. Such base flows, which are sheared vertically at the fixed bottom (also at fluid-fluid interfaces), can be disturbed by large-scale instabilities, for example introduced by islands. Large-scale eddy structures caused by such perturbations dominate the momentum and mass transport in the near-wake region. In such a shallow domain the flow field is recognized to deviate significantly from flow structures in an unbounded ambient. On one hand, purely kinematically, the reduced vertical dimension prevents a 3D decay of large vortical structures by secondary transverse instabilities. On the other hand, from dynamical grounds, bottom friction leads either to a complete suppression of the generation of large structures at the obstacle or to a downstream re-stabilization of the wake flow.

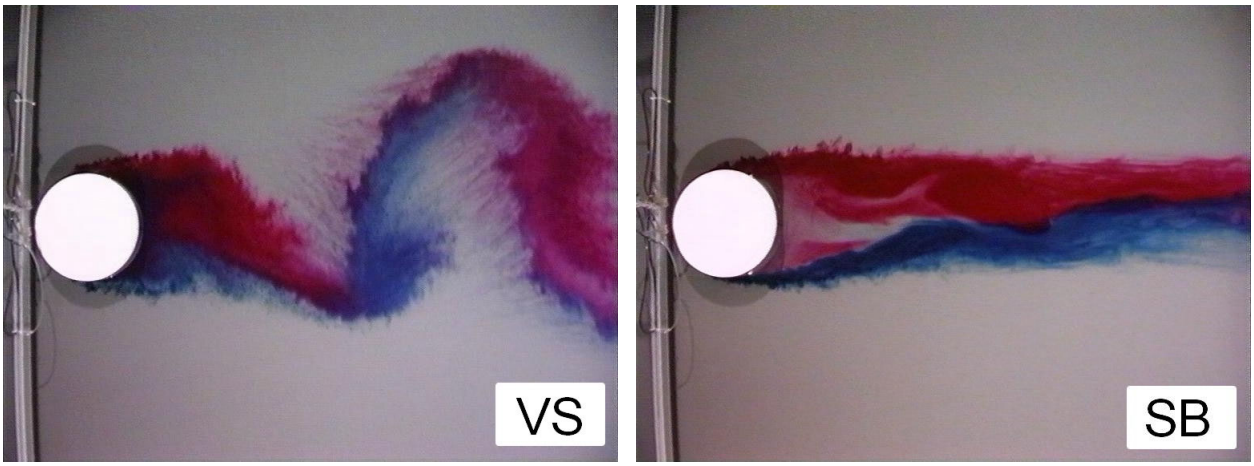

Fig. 1: Top view of different stability classes in shallow wake flows, visualized by dye injected at the upstream cylinder shoulders. The shallow vertical shear flow (from left to right) is horizontally sheared at a cylindrical body with a diameter several times the water depth. In the SB case large-scale instabilities, which can be induced by the horizontal shear (cf. VS case), are completely suppressed by bottom friction.

The study of wake flows behind cylindrical bodies in shallow turbulent shear flow contributes to the understanding of the genesis and preservation principles of the associated large-scale eddy structures and helps to quantify their transport characteristics for momentum and mass. Different instability mechanisms can be characterized regarding some of their large- and small-scale flow characteristics. A complete representation of the physical phenomena was given by CHEN & JIRKA (1995). A first type of stability ("Vortex Street" - VS) shows a formation which resembles a von Kármán vortex street, although here the cylinder Reynolds number Re_D is substantially larger than in the unbounded case. It is characterized by the alternate separation of large vortical structures directly from the cylinder shoulders which are then advected downstream and decay due to the continous influence of bottom shear. If, compared to the ambient flow conditions in the VS case, the stabilizing effect of bottom friction increases or the destabilizing transverse shear is reduced, the convectively unstable VS wake flow undergoes transition: an absolutely unstable recirculating region ("Unsteady Bubble" - UB) developes behind the obstacle, alternately large eddies shed from the downstream edge of the bubble and advect downstream until they disintregrate and the flow stabilizes. If the forcing due to transverse shear is even weaker, then genaration of large-scale vortices at the end of the recirculation zone is completely suppressed ("Steady Bubble" - SB). Nevertheless, the plane "mixing layers" forming the sides of the steady bubble nourish intermitant vortical structures, but they will disintegrate before they mature to the size of the mixing layer.

Experimental Set-Up and Measuring Techniques

For the analysis of the flow characteristics in such shallow shear flow two primary measurement techniques are used. First, the test facility is supplied with an improved combined Laser-Doppler Velocimetry and Laser Induced Fluorescence (LDV-LIF) technique, which allows for spacially well defined and temporally highly resolved synaptic data of velocity and mass fluctuations. Concerning the turbulence spectra in shallow cylinder wakes, details and results using LDV-LIF are reported in CARMER (2000) and CARMER & JIRKA (2001). Second, we employ a Particle Image Velocimetry (PIV) measuring system and an image analysis technique to gather horizontal velocity and tracer mass distributions. If we focus our interest on the development of quasi 2-D

large-scale eddies, whose chacteristic length and time scales are much larger than those of a plane shear flow, then we also need data with less temporal resolution, but spatially well resolved in a wide area of observation.

Particle Image Velocimetry. For the planar velocity measurements, a PIV system (LaVision) was employed to obtain and process video frames provided by a 12 bit, 1024 x 1280 pixel digital camera (PCO-SensiCam) with a frequency of 7 Hz. Using a 15 mm Nikon lense, undistorted pictures of the horizontal flow field in a 1.2 m wide and 1.4 m long area were captured. As tracer particles floating polypropylene beads (diameter 3 mm) were evenly distributed over the uniform flow upstream of the cylindrical obstacle and advected through the area of observation at the free surface. Because the flow velocities were slow and the floating particles defined the measurement plane of the PIV, we could omit using a laser-generated light-sheet. Typically, the 'adaptive multi pass' cross-correlation algorithm from the PIV system provided horizontal velocity fields on a regular 80 x 64 grid (spacing about 18 mm) with 7 Hz.

Planar Concentration Analysis. Depth-averaged scalar fields were obtained with a Planar Concentration Analysis (PCA) for the same flow configuration as the velocity fields, but not simultaneously, when food coloring was injected as a continuous single point-source at the upstream cylinder perimeter. Video images of the flow were taken in an area of 1.2 m x 1.6 m with 25 Hz and later digitized with a resolution of 3 x 8 bit and 768 x 576 pixels. Dye concentrations were calibrated with a set of background images recorded for identical flow depth and illumination. During the conversion of the gray-scale intensity images to concentration, which also took into account the nonlinear relation between light intensity and concentration, a spatial averaging (binning) was applied, finally resulting in scalar fields on a 170 x 128 grid (spacing 9.5 mm) with an effective concentration depth of about 6 bit. Details on the converting algorithm of the PCA as well as on the calibration procedure are given in Part 1 of this paper (RUMMEL ET AL., 2002).

Flow Conditions. Experiments were conducted for different flow regimes to span the different types of instability and their transition. Here we will present one series of measurements for a vortex street like cylinder wake with the following flow conditions: diameter of circular cylinder D = 125 mm, flow depth h = 18 mm, ambient velocity U_a = 0.130 m/s, Darcy-Weisbach bottom friction coefficient $\lambda = 2\ c_f$ = 0.0164. Reynolds numbers based on depth and diameter are Re_h = 2,340 and Re_D = 16,200. The flow is characterized by large eddies alternately separating from the left and right side of the cylinder.

Phase-Resolved Averaging and Structure Identification

Phase-Resolved Averaging. Since for this investigation the interest is also on the generation and downstream evolution of large-scale coherent vortical structures (LCS), these quasi 2-D vortices have to be identified and to be characterized due to the longitudinal development of typical properties. Therefore, the data has to be post-processed to provide sets of phase-resolved averaged vector and scalar fields. The general procedure of phase-resolved averaging makes use of the evident periodicity of the wake flow and implies the following steps. At first, the individual periods for each shedding cycle are determined for the velocity fields as well as for the concentration fields using an auto-correlation approach. Next, based on the individual cycle

periods, the time histories of the vector and scalar fields are re-organized by assigning each field of a time series to its appropriate phase angle φ. The cycle period is split into a number of phase intervals, and all fields belonging to a certain phase interval are then averaged, which leads to phase-resolved averaged fields for discrete phase angles. Using phase-resolved averaged instead of ensemble-averaged data, means to adopt a triple decomposition into mean, periodic and random parts, eg. $u_i(\vec{x},t) = U_i(\vec{x}) + u_{p,i}(\vec{x},\varphi) + u_{r,i}(\vec{x},t)$, instead of a classical Reynolds decomposition into mean and fluctuating parts. So, effectively the phase-resolved averaging procedure works like a narrow adaptive low-frequency bandpass-filter, which is adjusted to the individual frequency of each shedding cycle.

In addition, although no coincidentally sampled velocity and mass data is available from the planar measurements, we also want to study the mass transfer in the periodic, 'coherent' wake flow and the mass transport capacity of the LCS. Therefore, after adjusting the phase lag, both phase-resolved averaged fields of velocity and of tracer mass are finally cross-correlated.

Identification Scheme for Coherent Structures. Speaking of large coherent structures (LCS) we think of large-scale coherent vortical structures and follow a definition given by HUSSAIN (1986), p. 307: "A coherent structure is a connected [, large-scale] fluid mass with an instantaneously phase-correlated vorticity over its spatial extend." The general procedure to obtain the LCS is first to educe individual vortices from the time-resolved wake flow field, which are then averaged preserving phase information. In the case of a vortex street-like wake on the contrary, we first evaluate the phase-resolved average flow field from a time series. From this periodic 'coherent' flow we identify coherent eddy structures, which now are exactly the LCS.

For the identification of individual vortices, following MCWILLIAMS (1984), we make use of the Q values computed from the horizontal velocity fields. The Q function is defined as the difference of the squared strain terms and vorticity term given by

$$Q = \left(\frac{\partial u}{\partial x} - \frac{\partial v}{\partial y}\right)^2 + \left(\frac{\partial v}{\partial x} + \frac{\partial u}{\partial y}\right)^2 - \left(\frac{\partial v}{\partial x} - \frac{\partial u}{\partial y}\right)^2 \qquad (1)$$

Because the normal stress (first righthand term) is negligibly small compared to the shear stress (second term), the strain reduces to the shear strain and $-Q$ reduces to the second invariant of ∇u. Flow regions where $Q < 0$ are dominated by vorticity; whereas $Q > 0$ indicates strain dominated regions.

Vortex Street-Like Instability of a Shallow Turbulent Wake Flow

Phase-resolved averaging of velocity fields. Performing a resampling of the PIV data with a phase-resolved averaging of the time history of velocity fields means to extract the mean and periodic components of the flow $\{\vec{u}\} = \vec{U} + \vec{u}_p$. This 'coherent' part of the flow field is used to compute further quantities characterizing the large-scale low-frequency motion of the wake flow. We also use the 'coherent' flow to directly identify LCS in the wake flow without extracting any individual vortices. Making use of (1) we evaluate the spatial distributions of the Q value during the phase time. Moreover, we define a threshold value Q_{LCS} close to zero in order to distinguish the vorticity dominated regions from the wake flow. In Figure 2 we show a sequence of plots, which illustrate the evolution of LCS in the shallow turbulent wake of a cylindrical body. Here,

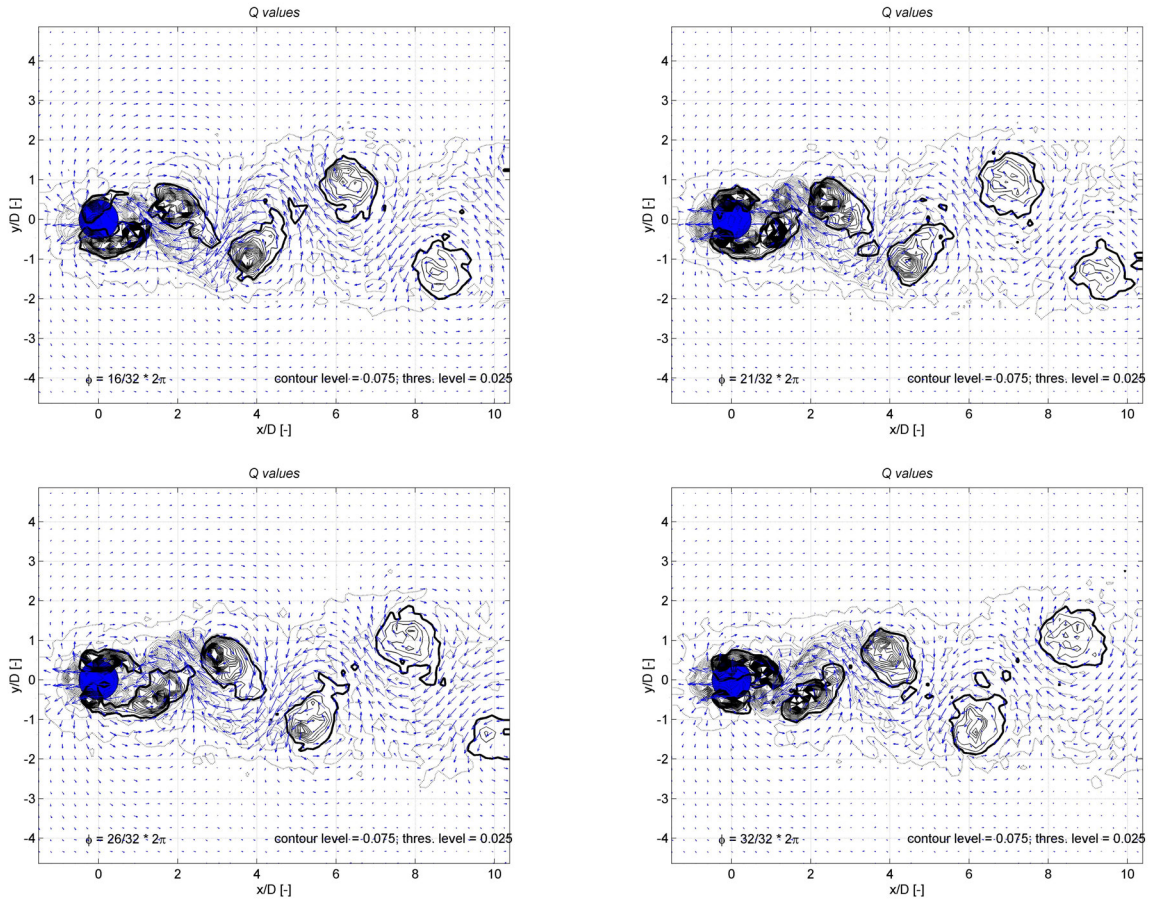

Fig. 2: Phase-resolved averaged horizontal flow fields of a vortex street-like instability of a shallow wake behind a cylindrical body. The ratio of cylinder diameter D and water depth h is $D/h = 7$, which indicates the shallowness of the flow. The 4 plots, taken from the second half of the phase cycle, illustrate the generation of a new LCS in the right wake shear layer. Vectors depict the phase-averaged flow reduced by the ambient flow velocity. Full contour lines show negative Q-values, i.e. vorticity dominated regions. The bold line marks a threshold value Q_{LCS} used to separate LCS from the shear dominated regions indicated by dotted contour lines.

full contour lines indicate vorticity dominated flow regions ($Q < 0$), whereas dotted lines show strain dominated regions. Bold full contour lines mark the small negative threshold value Q_{LCS}. Additionally, vectors indicate the phase-resolved averaged horizontal velocities $\{\vec{u}\}$ reduced by the ambient flow speed U_a for clarity. Obviously, vectors pointing towards the obstacle indicate the velocity deficit of the wake, but do not necessarily mean a recirculating flow.

From the velocity fields we can observe the vortex street-like behavior of the shallow wake flow. The boundary layers alternately roll up in the immediate lee of the cylinder, large vortical structures are stretched and finally separate. Then they are advected downstream forming a system of counter-rotating eddies in a staggered arrangement. Here, downstream of the obstacle, the initially streched LCS show their final, roughly circular shape. Their centers of rotation are shifted towards the outside of the wake, and they coincide with the local maxima of negative Q. With respect to the flow centerline, shear dominated regions are located axisymetrically opposite to the LCS, so separating the individual LCS and preventing them from merging. The saddle-points or sources of divergence, which play an important role in the development of vortex

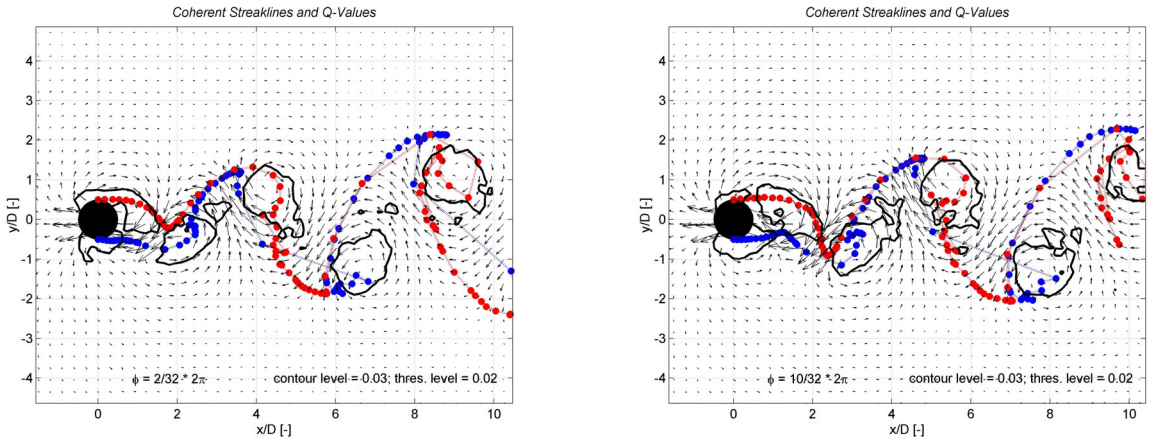

Fig. 3: Streaklines computed from the phase-resolved averaged flow fields are shown for two phase angles φ_i a quarter of a phase cycle apart. Further notation same as Fig. 2.

street-like flows, have the same longitudinal positions x/D as the local maxima of Q, and also as the centers of rotation of the LCS. Their lateral position depends on the velocity of the reference frame of observation, in the case of a frame moving with U_a the saddle points tend laterally towards infinity $(y/D \to \pm\infty)$.

Streaklines. From the phase-resolved averaged flow fields we can also compute streaklines to further elucidate the large scale periodic motion in the wake flow. In Figure 3 we show streaklines emerging from both sides of the cylindrical body. As the steaklines can be regarded as continuous releases of small tracer floats from point-sources, they can also provide an estimate for the mass transport solely by the LCS dominated low-frequency wake flow. The turbulent diffusive transport is excluded due to the filtering effect of the phase-resolved averaging procedure. We can observe very clearly the intrusion of ambient fluid across the whole wake and its final entrainment at the downstream ends of the LCS, where the strained braids connecting the LCS are rolled-up into the coherent eddies.

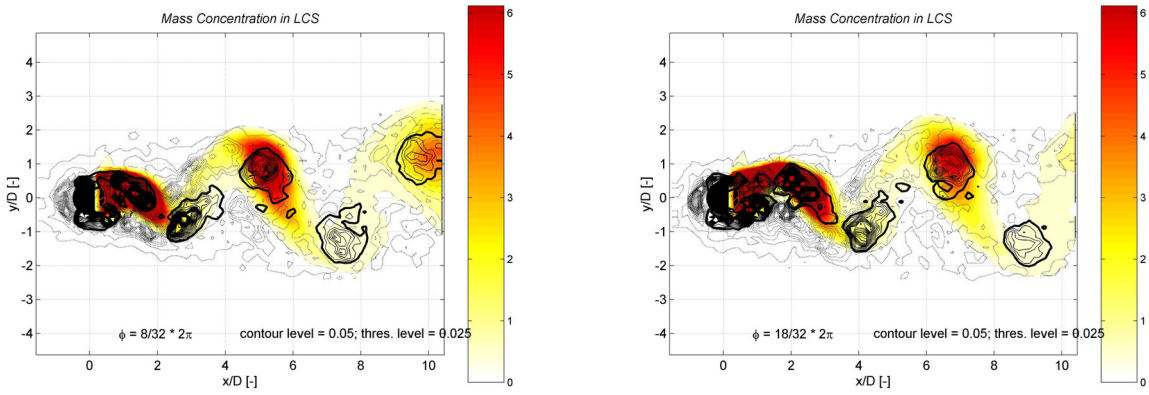

Fig. 4: A dye tracer is continuously injected from a point-source into the upstream left cylinder boundary layer. Color-coded we show the phase-resolved averaged mass concentration fields $\{c\}$ for two phase angles 1/3 of a phase cycle apart. Contour lines denote iso-values of Q (cf. Figure 2).

Phase-resolved averaged concentration fields. As a passive and conservative soluble tracer food coloring was introduced into the upstream left cylinder boundary layer from a continuous point-source. Using the PCA technique the depth-averaged mass concentrations $c(\vec{x},t)$ of the dye tracer were evaluated from grayscale intensity frames. These concentration fields then were phase-resolved averaged and cross-correlated to the velocity fields $\{\vec{u}\}$. Figure 4 shows the distribution of 'coherent' mass concentration $\{c\}$ for two different phase angles 1/3 of a phase cycle apart. Superimposed are the appropriate Q value distributions to indicate the LCS. As expected, the tracer mass is caught in the LCS and advected downstream primarily in the left line of eddies in the vortex street-like wake flow. Neither during the generation of LCS nor during their evolution, there is a significant exchange of mass between LCS of opposite rotation. Even though in the lee of the obstacle we observe a small region of high concentration, which is rather a low velocity layer than a recirculation zone, LCS detaching into the right side of the wake are not charged from this region. More downstream, tracer mass is transversely transferred from a LCS across the wake to the preceding counter-rotating eddy along the braid, which stretch away from the LCS. There it is wrapped around the vortex, then follows the next braid to reconnect to the adjacent LCS of the same sign. A similar transfer of mass along the braids is already visualized by the coherent steaklines in Figure 3, though the numeric floats are lined up along the braids only downstream of the LCS. The representation also of the small-scale turbulent shear stress, which smears out the thin coherent streak lines, should yield a distribution of floats similar to the mass concentrations, since the turbulent Schmidt number is of the order of unity.

Incoherent concentration fields. In order to get information about the entrainment of ambient fluid into the wake we could analyze the ensemble rms values of the whole time series of instantaneous concentration fields. More insight into the structural mechanisms of mixing can be obtained, if we evaluate the 'incoherent' fluctuating concentration fields. We therefore compute the standard deviations based on the phase-resolved averged concentration fields. Figure 5 exemplifies such phase-resolved rms values of mass concentrations for the same physical conditions and phase angles as used in Figure 4. The concentration fluctuations are cross-correlated to the LCS indicated by contour lines of Q values. In these plots we can identify regions of intense mixing, which are connected to the LCS. The most important mixing region is located near the outer side of the LCS just at the onset of the braid, where also the opposite

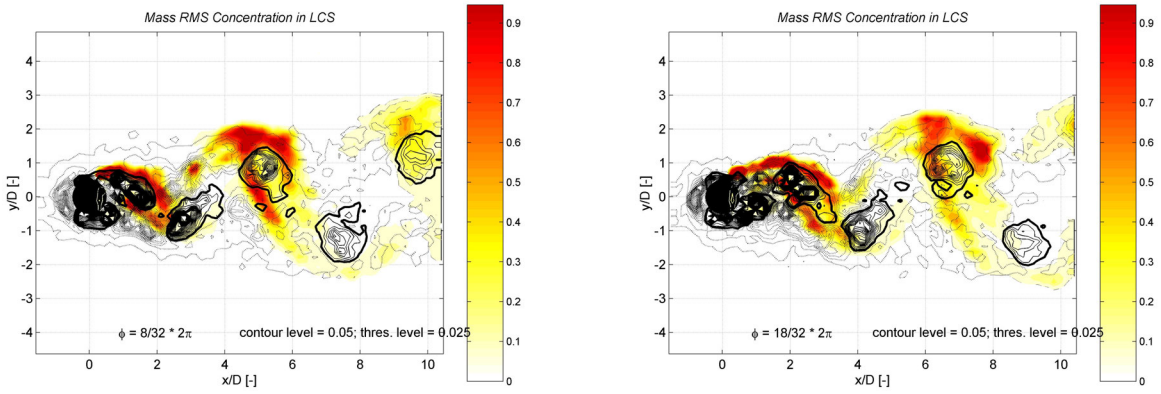

Fig. 5: The phase-resolved average fields of the rms values of the mass concentration $\{c_{rms}\}$ are displayed for the same conditions as in Figure 4.

coherent streakline folds back. Recalling the velocity fields we can state, that in this mixing region fresh fluid entraining from the other side of the wake is engulfed and incorporated into the LCS. A second region of high mixing is found upstream of the first one also near the outer boundery of the LCS. While the LCS is moving downstream, this region follows the rotation of the vortex core and moves in front of the vortex towards the wake centerline. Another filament of intense mixing is encountered, as the fresh fluid intrudes into the wake along the concentration-charged braid close to the downstream part of the LCS. Besides the identification of these mixing regions we also recognize areas showing almost no fluctuations. These are the cores of the LCS as well as the region in the immediate lee of the obstacle, which are also regions with the highest local magnitudes of mass concentration.

Mass transport due to large-scale structures. In the previous sections we presented low-frequency periodic distributions both of horizontal surface velocities obtained from PIV measurements and of depth-averaged mass concentrations from PCA for a vortex street-like shallow wake flow. Though the measurement techniques were not applied simultaneously and did not even span the same time history of the flow, the characteristic periodic flow pattern was extracted by phase-resolved average resampling. Subsequent cross-correlation enabled us to elucidate the topography of LCS and the associated mixing and entrainment. From the information obtained from the phase-resolved analysis, we can readily quantify the transfer of tracer mass within the wake flow. The standard triple decompostion of u and c, for example, yields the mean specific longitudinal mass flux

$$\langle cu \rangle = CU + \langle c_p u_p \rangle + \langle c_r u_r \rangle + \langle c_p u_r \rangle + \langle c_r u_p \rangle \qquad (2)$$

where the first three right-hand terms are the mean advective, large-scale periodic, and small-scale turbulent parts, respectively. The cross-correlated fluctuating parts are negligibly small, as the low- and high-frequency parts are almost completely decorrelated in vortex street-like shallow wake instability. Though the small-scale turbulent mass flux is not accessible by the PIV-PCA technique, as is applied here, we know from combined LDV-LIF measurements (cf. e.g. CARMER & JIRKA, 2001), that the small-scale turbulent axial mass transport rate is two

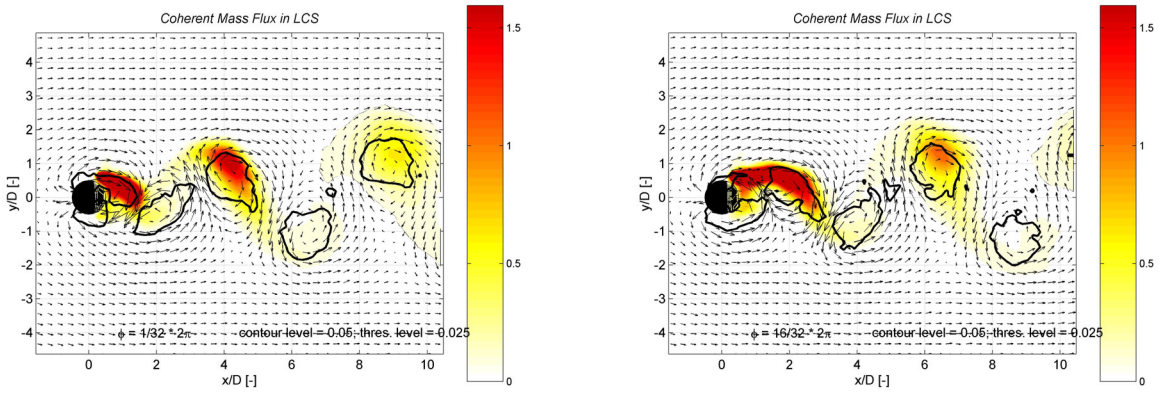

Fig. 6: The phase-resolved averaged distributions of the sum of absolute mean and large-scale mass fluxes $(C + c_p)\left|(\overrightarrow{U + u_p})\right|$ are displayed color-coded for two phase angles $\pi/2$ apart. The appropriate velocity vector fields are reduced by the mean eddy advection velocity U_{LCS}, and bold lines denote Q_{LCS} values to identify the LCS.

orders of magnitude smaller than the large-scale periodic transport and can thus be neglected.

In Figure 6 color-coded we show phase-resolved averaged distributions of the magnitude of the total mean and large-scale mass flux for two phase angles with a phase difference of $\pi/2$. Underlying we see bold lines of Q_{LCS} values and vector fields of phase-resolved average velocities reduced by the mean LCS advection speed U_{LCS}. It is obvious again, that the mass transport within the wake is related to the LCS, mass is mainly transferred within or close to the LCS. Also in the vortex cores, where the rotational velocity is small, a high mass flux is observed due to the mean vortex advection speed U_{LCS}. In Figure 7 we evaluated the longitudinal mass transport rate from the phase-resolved averaged flow fields for a similar vortex street-like wake denoted by blue circles and black crosses. Green squares show the same mass flux evaluated only from the LCS areas. Close to the cylinder almost 50 % of the flux takes place inside the LCS, then this fraction decreases, as the LCS disintegrate, whereas the total flux has to remain constant also far downstream. This demonstrates the restriction not only of the kinematic effects, but also of the dynamic influence of the LCS to a downstream distance of 20 to 30 diameters. Over this distance the LCS directly dissipate their kinetic energy, extracted from the mean flow at the obstacle, due to bottom friction. No down-cascading could be observed performing spectral analyses of LDV-LIF data.

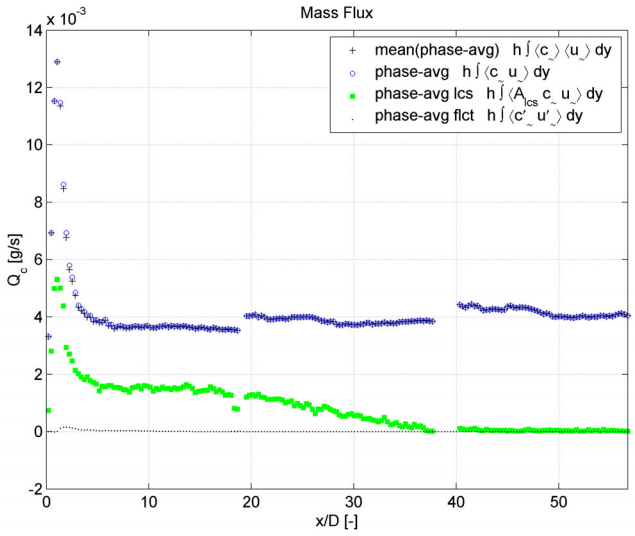

Fig. 7: The time-averaged low-frequency periodic longitudinal mass flux is evaluated for a similar vortex street-like shallow wake flow denoted by blue circles. The same quantity computed from areas covered by LCS only, are depicted as green squares.

Concluding Remarks

Planar measuring techniques for horizontal velocity and concentration fields have been adapted to shallow turbulent flows. Post-processing procedures to identify large-scale coherent vortical structures using their Q values and to evaluate their transport capacity for momentum and scalar properties from phase-averaged data have been developed. The topography of LCS arranged in a vortex street-like shallow wake flow elucidates the mechanisms of their generation and evolution. This has been examplified for the large-scale periodic entrainment and mixing of ambient fluid into the wake flow. Furthermore, 'coherent' mass transport rates, resolved both in spatial and in phase-time domain, have been computed from the cross-correlated fields. In order also to access the 'incoherent' mass transfer, we will soon present an improved PCA technique,

which allows to evaluate both velocity and concentration fields from the same raw video frames to provide substantially synaptic data. With such a coupled PIV-PCA technique for example also the turbulent diffusivity distribution can be related to the topography of the large-scale 'coherent' flow and to the LCS.

Acknowledgements

The support of the German Research Council (DFG grants Ji 18/4-2 and Ji 18/8-1) is acknowledged.

References

CARMER, C.F.V. (2000): LDA-LIF System zur Untersuchung großräumiger kohärenter Strukturen in flacher turbulenter Strömung. Delgado, A. et al. (Hrsg., 2000): Lasermethoden in der Strömungsmesstechnik. 8. GALA-Fachtagung. Shaker Verlag, Aachen.

CARMER, C.F.V. & JIRKA, G.H. (2001): On Turbulence and Transport in Shallow Wake Flows. Proceedings 29th IAHR Congress, Beijing, China.

CHEN, D. & JIRKA, G.H. (1995): Experimental study of plane turbulent wakes in a shallow water layer. Fluid Dyn. Res., 16:11-41.

HUSSAIN, A.K.F.M. (1986): Coherent structures and turbulence. J. Fluid Mech., 173:303-356.

MCWILLIAMS, J. (1984): The emergence of isolated coherent vortices in turbulent flow. J. Fluid Mech., 146:21-43.

RUMMEL, A.; CARMER, C.F.V.; JIRKA, G.H. (2002): Combined Planar Measurements of Flow Velocity and Mass Concentration in Shallow Turbulent Flow - Part 1: Development of a Planar Concentration Analysis (PCA) System. Proc. EWRI/IAHR International Conference on Hydraulic Measurements & Experimental Methods, Estes Park, USA.